Shape effects on the yield stress and deformation of silicon nanowires: A molecular dynamics simulation

Zhenyu Yang,[1] Zixing Lu,[1] and Ya-Pu Zhao[2,a)]
[1]*School of Aeronautical Science and Engineering, Beihang University, Beijing 100191, People's Republic of China*
[2]*State Key Laboratory of Nonlinear Mechanics, Institute of Mechanics, Chinese Academy of Sciences, Beijing 100190, People's Republic of China*

(Received 23 May 2009; accepted 27 June 2009; published online 31 July 2009)

The tension and compression of single-crystalline silicon nanowires (SiNWs) with different cross-sectional shapes are studied systematically using molecular dynamics simulation. The shape effects on the yield stresses are characterized. For the same surface to volume ratio, the circular cross-sectional SiNWs are stronger than the square cross-sectional ones under tensile loading, but reverse happens in compressive loading. With the atoms colored by least-squares atomic local shear strain, the deformation processes reveal that the failure modes of incipient yielding are dependent on the loading directions. The SiNWs under tensile loading slip in {111} surfaces, while the compressive loading leads the SiNWs to slip in the {110} surfaces. The present results are expected to contribute to the design of the silicon devices in nanosystems. © *2009 American Institute of Physics*. [DOI: 10.1063/1.3186619]

I. INTRODUCTION

Silicon nanowires (SiNWs) are known as the most important materials to the nanotechnology for its unique electronic, optoelectronic, thermal, and mechanical properties[1] and have thus attracted extensive research attention due to the wide application in microelectromechanical systems,[1] actuators and sensors,[2] memory devices,[3] transistors,[4] integrated circuits,[5] etc. The mechanical properties of the SiNWs are proved to be quite different from those of bulk materials due to their sizable surface area to volume ratio.[6] Relaxation and reconstruction in the silicon surfaces drastically affect their electronic properties.[7] As a result, the mechanical behaviors of the nanowires are also changed. Investigation on the mechanical properties is one of the key challenges that we need to overcome for the future technological applications of nanomaterials.

The mechanical properties of the single-crystalline SiNWs have been investigated by resonance testing,[8] ultrahigh-resolution electron microscope,[9] and atomic force microscopy (AFM) setup inside a scanning electron microscope (SEM).[10] Recently, Hsin *et al.*[11] reported using a manipulation probe and an AFM tip in SEM to investigate the mechanical behavior of a single SiNW under buckling and bending conditions, with some of the mechanical properties of SiNWs quantified. But such experiments cannot provide information on the defect evolution in plastic deformations. Characterizing the mechanical properties of individual nanowires is still a challenge to existing measuring techniques.

Menon *et al.*[12] investigated the stability and elastomechanical properties of tetragonal and cagelike or clathrate nanowires of silicon using molecular dynamics (MD) simulations with the Stillinger–Weber (SW) potential. Justo *et al.*[13] simulated the stability and plasticity properties of SiNWs using environment dependent interatomic potential model and characterized the effects of the cross-sectional shape on the mechanical properties of SiNWs. The first-principles calculation[14] revealed that Young's moduli of SiNWs are size dependent. In addition, the dislocation evolution in the silicon nanostructures has become increasingly attractive. Izumi and Yip[15] simulated the nucleation of a dislocation loop from a sharp corner on silicon and determined the activation energy and the saddle point configuration at low temperature. More recently, Godet *et al.*[16] investigated the onset plasticity of silicon nanostructures, with temperature and stress effects on the dislocation nucleation considered. However, despite the increasing volume of work on silicon nanostructures, information available about the plastic properties of SiNWs is lacking. A rigorous theoretical investigation of the structural, geometric, and mechanical properties of the SiNWs is necessary.

In this paper, MD simulations were employed to investigate the plastic properties of SiNWs with different cross-sectional shapes. Emphasis was placed on analyzing the propensity of the SiNWs to deform by slip. The cross-sectional shape effects were characterized. The mechanisms of the defect activation in tensile and compressive loading were discussed, respectively. The atomic local shear strain was used to detect the movement of the defects inside the nanowires and was correlated with the mechanical deformation of the nanowires. A deep understanding to plasticity, stability, and deformation of the SiNWs was achieved.

II. SIMULATION METHODS

We investigated the structure and mechanical properties of single-crystalline SiNWs using MD simulations with the SW many-body potential[17] for Si–Si interactions, which has been successfully used in simulation of fracture[18] and dislo-

[a)]Author to whom correspondence should be addressed. Electronic mail: yzhao@imech.ac.cn.

 © 2009 American Institute of Physics

Author complimentary copy. Redistribution subject to AIP license or copyright, see http://jap.aip.org/jap/copyright.jsp

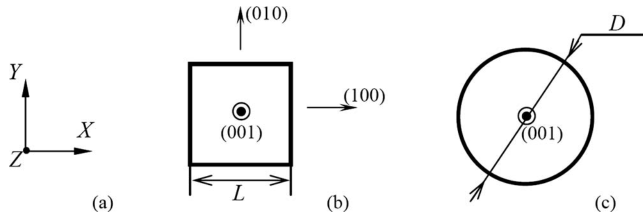

FIG. 1. The cross-sectional shapes of the nanowires considered in this paper. (a) The coordinates. (b) Square cross section with lateral dimension of L. (c) Circular cross section with diameter of D. L was set to be equal to D to keep the nanowires in the same surface area to volume ratio.

cation nucleation in silicon nanostructures.[16] The empirical SW interatomic potential consists of two- and three-body interaction terms and was originally fitted to describe the crystalline and liquid silicon phases.[19] Based on the experiments,[1,4,6] the as-grown SiNWs can be aligned along [100], [110], and [111] directions with lateral dimension ranging from 1 to 10^2 nm. In this study, we focused on [100] oriented SiNWs. The nanowire models with different cross-sectional shapes were cut from the diamond-cubic crystal silicon. Here, the SiNWs with square and circular cross sections were considered (Fig. 1), which were abbreviated to S-SiNWs and C-SiNWs, respectively. To make two types of nanowires in the same surface area to volume ratio, the lateral dimension of S-SiNWs L was set to be equal to the diameter of the C-SiNWs D. In order to save computational time, the SiNWs considered in this work are relatively thin, with L and D equal to 12 cubic lattice units (CLUs). The nanowires are relaxed to a minimum energy configuration with all free boundary conditions, and then thermally equilibrated to 300 K for 50 ps using the Nosé–Hoover thermostat[20] with a time step of 2 fs and keeping the length of the wires constant. Approximation to quasistatic tensile loading[21,22] in each deformation increment is achieved in two steps, including a 10 ps loading process and a 10 ps relaxation. The loading is applied along the axis of the nanowires, with the bottom layers fixed, while the rest of the atoms were displaced in accordance with a prescribed uniform strain in the length direction. Periodic boundary conditions were not used at any direction for all the simulations in this work. The velocity Verlet algorithm[23] was used to integrate the equations of motion, and all MD simulations in this study were performed using the parallelized code LAMMPS.[24] The stresses reported in this work were calculated using the virial theorem, which is equivalent to the Cauchy stress in the average sense.[25] The snapshots of the MD results were processed by the package of ATOMEYE.[26]

For the purpose of quantifying plastic deformation of the nanowires at the atomic level and viewing defect evolution in nanowires, colors are assigned to the atoms according to atomic local shear strain[27] η_i^{Mises}, which is also called annotate atomic strain. Calculation of η_i^{Mises} requires two atomic configurations, one current and one reference. The relative position vector $\mathbf{r}_{ij}^0$ between atoms j and i in perfect lattice structure is transformed into $\mathbf{r}_{ij}$ by a local transformation matrix $\mathbf{J}_i$. The local Lagrangian strain matrix of atom i is then calculated as

$$\boldsymbol{\eta}_i = \tfrac{1}{2}(\mathbf{J}_i\mathbf{J}_i^T - \mathbf{I}). \tag{1}$$

The local shear invariant of atom i can be computed as

$$\eta_i^{\mathrm{Mises}} = \sqrt{\eta_{yz}^2 + \eta_{xz}^2 + \eta_{xy}^2 + \tfrac{1}{6}[(\eta_{yy}-\eta_{zz})^2 + (\eta_{xx}-\eta_{zz})^2 + (\eta_{xx}-\eta_{yy})^2]}. \tag{2}$$

A cutoff is used to separate the first and second nearest neighbors in a perfect crystalline lattice. This scheme works extremely well in practice,[27] allowing one to directly visualize microstructures, including point defects, dislocations, stacking faults, and their strain fields with color encoding.

III. SIMULATION RESULTS AND DISCUSSIONS

A. Shape effects on the yield stress

The relaxation and reconstruction on the surfaces of nanomaterials can lead to size-dependent mechanical responses,[28] including Young's modulus and yield strength. The elastic properties of SiNWs have been frequently studied in the literatures.[14,29,30] Because of the abundance of prior works on this orientation, we here focus on the yield strength and the plastic deformation of SiNWs.

For comparison, the S-SiNWs and C-SiNWs are created with the same surface area to volume ratio and aspect ratio of 3. The representative stress-strain curves for the two types of nanowires with a lateral dimension of 12 CLUs, which are subjected to uniaxial tensile and compressive loadings at $T = 300$ K, are shown in Fig. 2. For the tensile loading, the elastic limit of C-SiNW is 11.10%, which is higher than that of S-SiNW, 10.80%. The tensile deformations are almost linear for both nanowires. However, for the compressive loading, the S-SiNW yields at a strain of 10.85% and C-SiNW at 9.75%. The compressive deformations are obviously nonlinear and the stress-strain curves exhibit larger nonlinear characters as the yield points are approached. Both nanowires deform elastically until yielding. A recent experiment[31] shows that the Si crystalline nanostructures can be strained up to more than 12%, which is comparable with the presented simulations.

As can be seen, the yield stresses for the S-SiNW are 11.06 and 8.89 GPa, respectively, for tension and compression. For the C-SiNWs, the corresponding values are 11.21 and 8.05 GPa. The shape-induced yield stress difference for tension is 0.15 GPa and it is 0.83 GPa for compression. Although the shape effects on yield stresses of SiNWs are

Author complimentary copy. Redistribution subject to AIP license or copyright, see http://jap.aip.org/jap/copyright.jsp

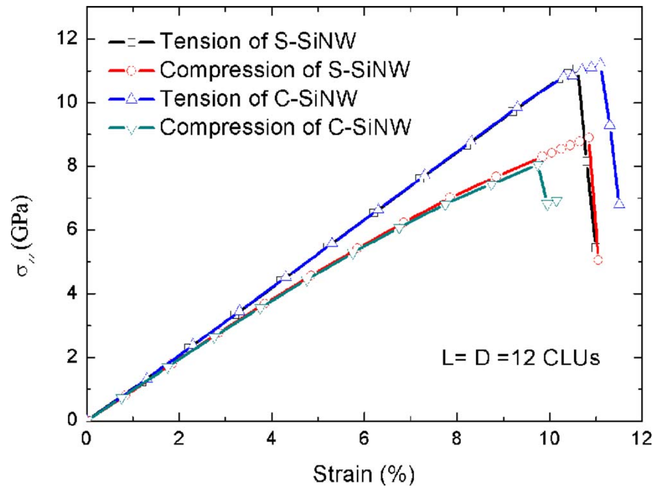

FIG. 2. (Color online) Representative stress-strain curves for the SiNWs with different cross-sectional shapes subjected to uniaxial tensile and compressive loadings at 300 K. The lateral dimensions of the samples are 12 CLUs.

not as strong as that on the metal nanowires (3.4 GPa),[21] these effects cannot be neglected. According to Fig. 2, the asymmetry of the yield stress can also be found. The yield stress difference between the tension and compression is 2.71 GPa for S-SiNWs, and the value is 3.16 GPa for C-SiNWs. The difference between the yield strength for tension and compression of nanowires has been attributed to the effects of surface stress.[22,32] For nanowire, the surface stress existing on the surfaces can induce intrinsic stresses in the interior of the nanowire, which leads to yield stress asymmetry. As a result, the magnitude of the tensile yield stress is larger than that of the compressive yield stress for both SiNWs.

B. Local shear strain in the surface

The distribution of local shear strain on the cross sections after equilibrium at $T=300$ K was evaluated for the two types of nanowires, which are shown in Figs. 3 and 4, respectively. Figures 3(a) and 4(a) show the initial configurations of the nanowires before they are cut from the silicon bulk. Comparing Figs. 3(a) and 3(b), the $p(2\times1)$ reconstruction[33] on the side surface of S-SiNW can be observed from the side view, where the structure of surface atoms on the {100} plane is obviously reconstructed. As can be seen from Figs. 3(c) and 3(d), the shear strain is maximum at the outmost surface atomic layers because the atoms near the surface are exposed to different forces from those in the interior of the material. The atoms near the surface tend to minimize the total free energy by relaxation mostly perpendicular to the surface (not shown here) and reconstruction parallel to the surface, which also leads the surface stress to be changed. For the cylindrical nanowire, the reconstruction in the surface also leads to maximum strain at the surface atoms, as shown in Figs. 4(c) and 4(d). Kang and Cai[18] also observed reconstruction of surface atoms with SW potential at 300 K and the maximum displacements of the surface atoms are given. With Figs. 3(d) and 4(d), it can be observed that only the upmost two to three layers of the atoms are involved in the surface effects, which indicate the dominating range of the surface effects. This observed phenomenon illuminates the modeling of the nanostructures based on continuum mechanics.

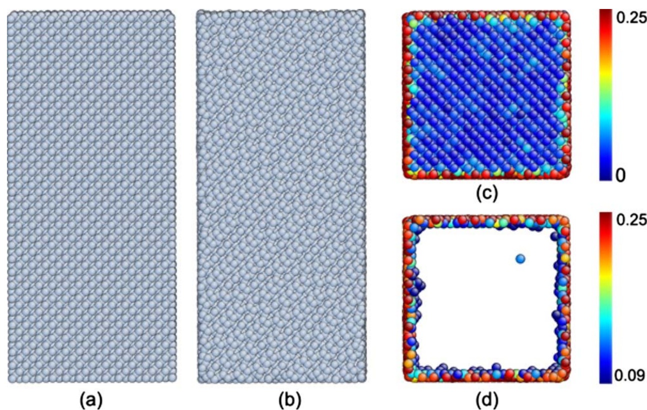

FIG. 3. (Color online) The distribution of local shear strain on S-SiNWs, which is induced by surface reconstruction. (a) Nanowire before equilibrium. (b) The nanowire with surface reconstructed. (c) Sectional view along the axis; the atoms are colored with local shear strain ranging from 0 to 0.25. (d) Atoms with local shear strain ranging from 0.09 to 0.25, where only the surface atoms show.

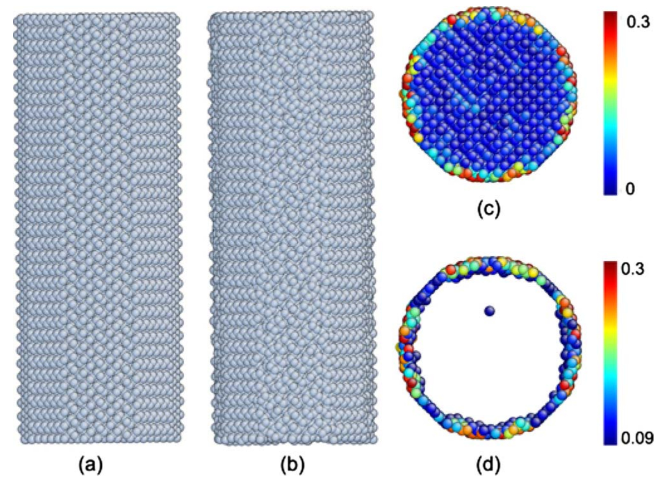

FIG. 4. (Color online) The distribution of local shear strain on C-SiNWs. (a) Nanowire before equilibrium. (b) The nanowires after surface reconstruction. (c) Sectional view along the axis; the atoms are colored with local shear strain ranging from 0 to 0.30. (d) Atoms with local shear strain ranging from 0.09 to 0.30, where only the surface atoms show.

C. Deformation of SiNWs via slip

In this section, we present numerical simulations of uniaxial tension and compression of the (001) nanowires, including S-SiNWs and C-SiNWs. By monitoring the deformation snapshots, we observe the onsets of plasticity via the slip planes. Here, for clarity, only the typical deformation snapshots of S-SiNWs are given. In fact, both nanowires have the same slip systems as the SiNWs are in the same loading status. Figure 5 shows the deformation process of the S-SiNWs with a lateral dimension of 12 CLUs under uniaxial tensile loading. The dislocation nucleation at the surface can be observed in Fig. 5(a), which is the snapshot of elastic limit. As the strain increases further, the SiNW yields with a slip plan emerging [Fig. 5(b)]. Coloring by local shear

Author complimentary copy. Redistribution subject to AIP license or copyright, see http://jap.aip.org/jap/copyright.jsp

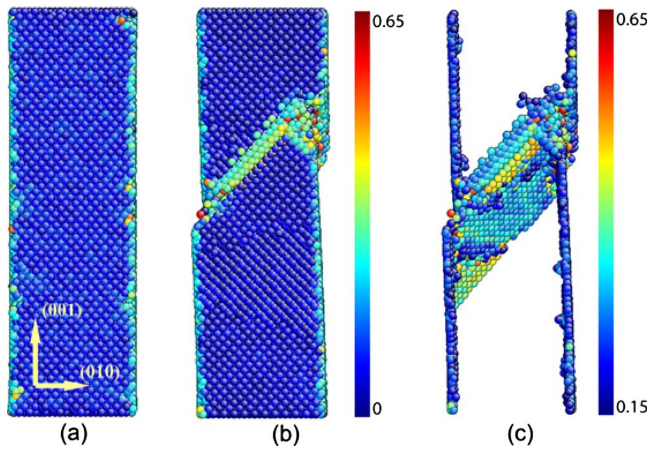

FIG. 5. (Color online) Snapshots of deformation of S-SiNW with a lateral dimension of 12 CLUs at initial yield under tensile loading. (a) Sectional view along (100) at elastic limit. (b) Sectional view of the initial yield configuration. (c) The slip planes at the initial yield. The surface atoms are removed for clarity.

strain, the slip plane inside the nanowire is identified to be a $\{\bar{1}\bar{1}1\}$ plane. To see the inside structure distinctly, the atoms with a local shear strain below 0.15 and the atoms in anterior and posterior surfaces are removed to display only the shear band, as shown in Fig. 5(c). The dislocation that nucleates in the $\{\bar{1}\bar{1}1\}$ slip plane is characterized by a Burgers vector $\vec{b} = 1/2[011]$. Extensive sliding over this plane leads to significant deformation of the cross section before the eventual fracture. The phenomenon is in agreement with what Godet *et al.*[16] observed in other silicon nanostructures with large stress. In addition, the thickness of the shear band is estimated to be three to four atomistic layers with relaxed atom surrounding, as shown in Fig. 5(c). For the C-SiNWs, the deformation process is similar and the shape of the slip plane is elliptical, which is not shown here. The more details of defect evolution are shown in Fig. 6 by viewing from the axis direction and atoms being colored with local shear strain. The propagation of the slip is observed to initiate at the corner of the nanowire, as shown in Fig. 6(b). A recent

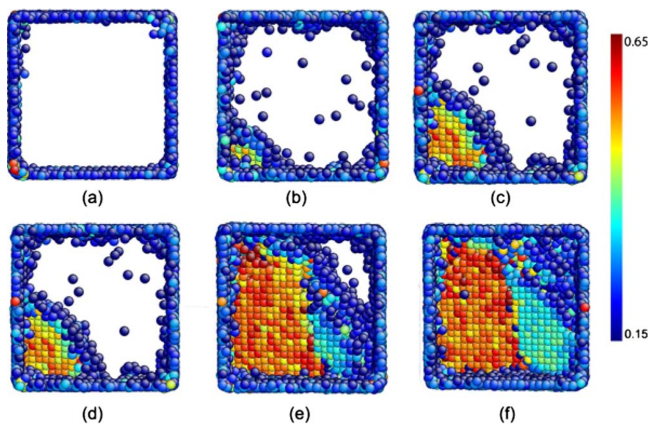

FIG. 6. (Color online) Snapshots of defect evolution inside the S-SiNW under tensile loading along the nanowire axis. (a) The inside structure before loading. The dislocation nucleates from the edge corner of the SiNW in (b) and propagates along the $\{\bar{1}\bar{1}1\}$ plane in (c)–(e), eventually creating a surface step in (f). The atoms are colored by the atomic local shear strain.

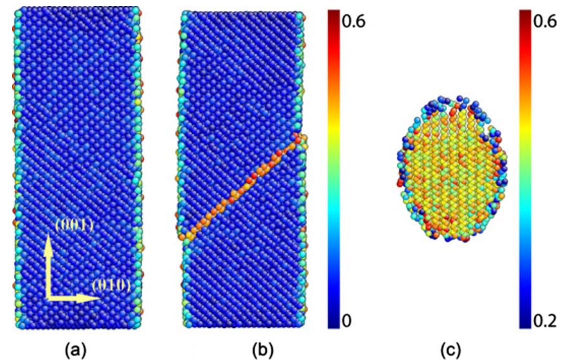

FIG. 7. (Color online) Snapshots of compressive deformation of the C-SiNWs with a diameter of 12 CLUs. (a) Sectional view along (100) at elastic limit. (b) The initial yield. (c) The snapshot of the slip plane from the $(0\bar{1}1)$ direction at the same strain level with (b).

analysis[34] based on reaction pathway modeling of dislocation nucleation revealed that the activation energy for the nucleation from the side surface is far higher than that of the nucleation from the corner. MD simulations[21] on the uniaxial loading of Cu nanowires also show that the dislocations prefer to nucleate at the corner. So the nucleation from the corners dominates over the surface sources and the corner nucleation is confirmed as a favored mode. A similar dislocation was also found to nucleate from a sharp corner by Izumi and Yip.[15]

For the cases of compressive loading, snapshots of the representative deformation process of the 12 CLU C-SiNWs can be seen in Fig. 7. For clarity, the snapshots of S-SiNWs under compressive loading are not shown here because the nanowires with different cross-sectional shapes show the same slip systems. In comparison to the tensile deformation, the compressive deformation shows some different characteristics. As far as the stress strain curves (Fig. 2), the SiNWs under compressive loading deform nonlinearly, while the SiNWs under tensile loading deform linearly. In addition, the failure mode of SiNWs under compressive loading is found to be different with aforementioned that of tensile loading. When the stress reached the critical value, sliding occurs in a $\{0\bar{1}1\}$ plane. Based on the snapshots of deformation, the slip plane in C-SiNW under compressive loading is shown in Fig. 7(c). Further analysis reveals that the first slip event is initiated by the nucleation of a dislocation half loop from the surface and propagates in the $(0\bar{1}\bar{1})$ direction, as shown in Fig. 8. A MD simulation on (110) SiNWs by Kang and Cai[18] revealed that the crack initiates from the surface of the nanowire and propagates along the (110) plane. The *ab initio* calculation[35] also predicted that cracks can be driven on a {110} plane. We found that the nanowire's fracture is triggered by extensive dislocation slip activities and can be considered as a ductile fracture, which is also dependent on the atomistic potential.[18] The predominant compressive deformation mechanism is slip via partial dislocation nucleation; this is evident by the slip system observed along the $\{0\bar{1}1\}$ plane in Figs. 7 and 8. The thickness of the slip plane characterized by local shear strain is about two atomistic layers, which is thinner than that of slip plane in uniaxial tensile loading.

Author complimentary copy. Redistribution subject to AIP license or copyright, see http://jap.aip.org/jap/copyright.jsp

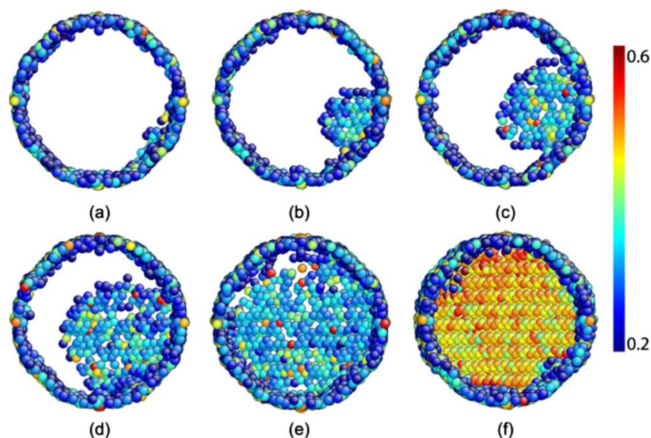

FIG. 8. (Color online) Snapshots of defect evolution inside the C-SiNW under compressive loading along the nanowire axis. At low strain, no nucleation of dislocation in (a). As the strain increases further, dislocation nucleates at the surface in (b) and propagates along the $\{0\bar{1}1\}$ plane in (c)–(e), eventually creating a surface step in (f). The atoms are colored by the atomic local shear strain.

D. Discussions

With neglecting the contribution of the surface elasticity, the effective yield stress[22,36] of the nanowire was related to the surface stress τ by $\sigma_e = (2/a)\tau \pm \sigma_y$, where a is the lateral dimension and σ_y is the ideal yield strength of the bulk material. Based on this continuum theory, the asymmetry of the yield stress is the result of the surface stress. According to Fig. 2, the effects of surface stress on the C-SiNWs are more obvious than that on the S-SiNWs. From the point of strain, the outmost surface atomic layer is highly defective with high strain, as shown in Figs. 3 and 4. For metal nanowires,[21] the dislocation nucleates at a sharp corner of the square surface, which is not present on the circular surface, and the local shear strain distributions on the surfaces were proved to be a significant factor in controlling the dislocation nucleation. Actually, for the SiNWs, the comments apply equally here. The barrier for dislocation nucleation is much smaller than the flat surface,[34] and the cross-sectional shapes influence the required stress for dislocation nucleation,[21] which is regarded as the major cause of the shape effects.

In addition, the slip behavior involved in tension and compression can be understood from a Schmid factor analysis. Schmid factor of a slip system is $m = \cos\varphi \cos\lambda$, where φ is the angle between the normal of the slip plane and the direction of the applied force and λ is the angle between the slip plane direction and the direction of the applied force. The uniaxial Schmid factor for the slip systems in the (001) SiNWs is larger under compression (0.5) than under tension (0.41), and thus makes it easier for the nanowires to yield under compression, which is consistent with the previous observation on the stress-strain relationships. Further, the critical resolved shear stress (CRSS) is given by $\tau = \sigma_y \cos\varphi \cos\lambda$, where σ_y is the magnitude of the yield stress. The calculated CRSS is larger for tensile yielding (4.51 and 4.57 GPa for S-SiNW and C-SiNW, respectively) than compressive yielding (4.45 and 4.03 GPa), which indicates that the slip system in compression is easier to be activated. These two factors can also contribute to the significant tensile/compressive yield stress asymmetry (Fig. 2) in (001) SiNWs.

Silicon was reported to have two principal cleavage planes:[35,37] {111} planes, usually the easy cleavage planes, and {110} planes. In this work, the calculations show that {111} planes are the predominant planes for the SiNWs under tensile loading, while {110} planes are especially for the SiNWs under compressive loading. For the cleavage planes, surface energies given by the modified potential[38] are 1.33 $\mathrm{J/m^2}$ for the unreconstructed Si (111) surface and 1.56 $\mathrm{J/m^2}$ for the unreconstructed (110) surface, and the density functional theory calculation gives surface energies ($\gamma_{110} \sim 1.7\ \mathrm{J/m^2}$ and $\gamma_{111} \sim 1.4\ \mathrm{J/m^2}$),[35] which are close to the range of experimental values[39] [1.23 $\mathrm{J/m^2}$ for the (111) surface and 1.51 $\mathrm{J/m^2}$ for the (110) surface]. All the data indicate that the energy to activate the {111} slip planes is lower than that of {110} slip planes. An *ab initio* study[35] also proved that cracks in silicon propagate easily on {111} and {110} planes provided crack propagation proceeds in the $(\bar{1}10)$ direction. Based on the simulations of the SiNW's uniaxial tension, Kang and Cai[18] found that the fracture behavior is the result of the competition between two different failure modes: cleavage on the (110) plane and slip on the (111) plane. These findings obtained by other methods corroborate our simulation results. The plastic transition between the glide and the shuffle set was proved to be dependent on the temperature and the applied stress.[16] Here, our results show that the deformation mode is dependent on the loading direction. Beyond this, the temperature and strain-rate effects on the SiNW's plastic deformation can be investigated further, which are not considered in the present work.

IV. CONCLUSIONS

In summary, MD simulations in room temperature have been employed to study the mechanical behaviors of single-crystalline SiNWs with different shapes under tensile and compressive loadings. The atomic local shear strains on the free SiNWs reveal that the uppermost two to three layers of surface atoms may represent the range of the surface effects. The strains retained in nanowires can significantly affect their electronic properties by perturbing the band structure or changing the Fermi energy of the nanostructures,[40] as well as the mechanical properties are changed. The snapshots of deformation show that the plastic deformation mechanism of single-crystalline SiNWs is slip via dislocation nucleation at surfaces. For the nanowires with the same surface to volume ratio, the cross-sectional shapes of the nanowires can affect the mechanical behaviors, leading to the differences in yield strengths. The stress-strain relationships for the tension and compression of SiNWs are proved to be asymmetric, which can be attributed to the surface effects. In addition, the failure modes for the SiNWs under tensile and compressive loadings are found to be different. The {111} slip plane is activated in tension of SiNWs, while the {110} slip plane is activated in compression loading, which shows that the predominate slip planes are determined by the stress status. This

Author complimentary copy. Redistribution subject to AIP license or copyright, see http://jap.aip.org/jap/copyright.jsp

result is expected to provide insight into the plastic deformation mechanism in nanoscale semiconductor devices.

ACKNOWLEDGMENTS

Z.Y. was supported by the China Postdoctoral Science Foundation under Grant No. 20080440013 and Z.L. was supported by the Common Construction Project of Education Committee of Beijing under Grant No. XK100060522. Y.-P.Z. was supported by the NSFC (Grant Nos. 10772180 and 10721202), the National Basic Research Program of China (973 Program, Grant No. 2007CB310500), and the National High-tech R&D Program of China (863 Program, Grant Nos. 2007AA04Z348 and 2007AA021803).

[1]J. D. Holmes, K. P. Johnston, R. C. Doty, and B. A. Korgel, Science **287**, 1471 (2000).
[2]Y. Cui, Q. Q. Wei, H. K. Park, and C. M. Lieber, Science **293**, 1289 (2001).
[3]H. T. Chen, S. I. Hsieh, C. J. Lin, and Y. C. King, IEEE Electron Device Lett. **28**, 499 (2007).
[4]Y. Cui, Z. H. Zhong, D. L. Wang, W. U. Wang, and C. M. Lieber, Nano Lett. **3**, 149 (2003).
[5]M. Law, J. Goldberger, and P. Yang, Annu. Rev. Mater. Res. **34**, 83 (2004).
[6]D. D. D. Ma, C. S. Lee, F. C. K. Au, S. Y. Tong, and S. T. Lee, Science **299**, 1874 (2003).
[7]R. Rurali and N. Lorente, Nanotechnology **16**, S250 (2005).
[8]X. X. Li, T. Ono, Y. L. Wang, and M. Esashi, Appl. Phys. Lett. **83**, 3081 (2003).
[9]X. D. Han, K. Zheng, Y. F. Zhang, X. N. Zhang, Z. Zhang, and Z. L. Wang, Adv. Mater. (Weinheim, Ger.) **19**, 2112 (2007).
[10]S. Hoffmann, I. Utke, B. Moser, J. Michler, S. H. Christiansen, V. Schmidt, S. Senz, P. Werner, U. Gosele, and C. Ballif, Nano Lett. **6**, 622 (2006).
[11]C. L. Hsin, W. J. Mai, Y. D. Gu, Y. F. Gao, C. T. Huang, Y. Z. Liu, L. J. Chen, and Z. L. Wang, Adv. Mater. (Weinheim, Ger.) **20**, 3919 (2008).
[12]M. Menon, D. Srivastava, I. Ponomareva, and L. A. Chernozatonskii, Phys. Rev. B **70**, 125313 (2004).
[13]J. F. Justo, R. D. Menezes, and L. V. C. Assali, Phys. Rev. B **75**, 045303 (2007).
[14]B. Lee and R. E. Rudd, Phys. Rev. B **75**, 195328 (2007).
[15]S. Izumi and S. Yip, J. Appl. Phys. **104**, 033513 (2008).
[16]J. Godet, P. Hirel, S. Brochard, and L. Pizzagalli, J. Appl. Phys. **105**, 026104 (2009).
[17]F. H. Stillinger and T. A. Weber, Phys. Rev. B **31**, 5262 (1985).
[18]K. Kang and W. Cai, Philos. Mag. **87**, 2169 (2007).
[19]H. Balamane, T. Halicioglu, and W. A. Tiller, Phys. Rev. B **46**, 2250 (1992).
[20]S. Nose, J. Chem. Phys. **81**, 511 (1984).
[21]A. Cao and E. Ma, Acta Mater. **56**, 4816 (2008).
[22]Z. Y. Yang, Z. X. Lu, and Y. P. Zhao, Comput. Mater. Sci. **46**, 142 (2009).
[23]L. Verlet, Phys. Rev. **159**, 98 (1967).
[24]S. Plimpton, J. Comput. Phys. **117**, 1 (1995).
[25]K. S. Cheung and S. Yip, J. Appl. Phys. **70**, 5688 (1991).
[26]J. Li, Modell. Simul. Mater. Sci. Eng. **11**, 173 (2003).
[27]F. Shimizu, S. Ogata, and J. Li, Mater. Trans. **48**, 2923 (2007).
[28]J. G. Guo and Y. P. Zhao, J. Appl. Phys. **98**, 074306 (2005).
[29]R. E. Miller and V. B. Shenoy, Nanotechnology **11**, 139 (2000).
[30]T. Kizuka, Y. Takatani, K. Asaka, and R. Yoshizaki, Phys. Rev. B **72**, 035333 (2005).
[31]K. C. Lu, W. W. Wu, H. W. Wu, C. M. Tanner, J. P. Chang, L. J. Chen, and K. N. Tu, Nano Lett. **7**, 2389 (2007).
[32]J. K. Diao, K. Gall, and M. L. Dunn, Nano Lett. **4**, 1863 (2004).
[33]D. J. Chadi, Phys. Rev. Lett. **43**, 43 (1979).
[34]T. Zhu, J. Li, A. Samanta, A. Leach, and K. Gall, Phys. Rev. Lett. **100**, 025502 (2008).
[35]R. Pérez and P. Gumbsch, Acta Mater. **48**, 4517 (2000).
[36]W. X. Zhang, T. J. Wang, and X. Chen, J. Appl. Phys. **103**, 123527 (2008).
[37]J. Li, A. H. W. Ngan, and P. Gumbsch, Acta Mater. **51**, 5711 (2003).
[38]J. G. Swadener and S. T. Picraux, J. Appl. Phys. **105**, 044310 (2009).
[39]R. J. Jaccodine, J. Electrochem. Soc. **110**, 524 (1963).
[40]D. Tekleab, D. L. Carroll, G. G. Samsonidze, and B. I. Yakobson, Phys. Rev. B **64**, 035419 (2001).

Author complimentary copy. Redistribution subject to AIP license or copyright, see http://jap.aip.org/jap/copyright.jsp